nature materials

SUPPLEMENTARY INFORMATION

DOI: 10.1038/NMAT3963

Optically enhanced coherent transport in $YBa_2Cu_3O_{6.5}$ by ultrafast redistribution of interlayer coupling

W. Hu[1*], S. Kaiser[1*], D. Nicoletti[1*], C.R. Hunt[1,4*], I. Gierz[1], M. C. Hoffmann[1], M. Le Tacon[2], T. Loew[2], B. Keimer[2], and A. Cavalleri[1,3]

[1] *Max Planck Institute for the Structure and Dynamics of Matter, Hamburg, Germany*
[2] *Max Planck Institute for Solid State Research, Stuttgart, Germany*
[3] *Department of Physics, Oxford University, Clarendon Laboratory, Oxford, United Kingdom*
[4] *Department of Physics, University of Illinois at Urbana-Champaign, Urbana, Illinois, USA*

S1 Sample Growth and Characterization

$YBa_2Cu_3O_{6+\delta}$ crystals of typical dimensions 2 x 2 x 1 mm^3 were grown in Y-stabilized zirconium crucibles[1]. The hole doping of the Cu-O planes was adjusted by controlling the oxygen content of the CuO chain layer δ by annealing in flowing O_2 and subsequent rapid quenching. A sharp superconducting transition at T_c = 50 K (ΔT_c~2 K) was determined by *dc* magnetization measurements, as shown in Figure FS1.1A.

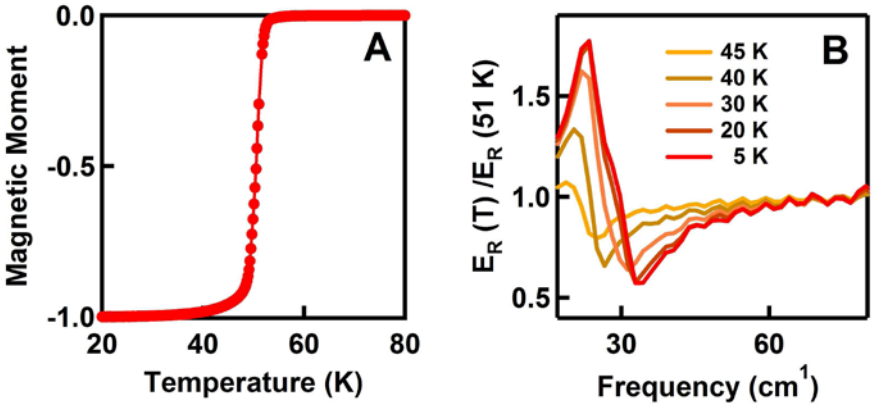

Figure FS1.1 (A) SQUID characterization of the dc magnetization across the superconducting transition. **(B)** Josephson plasma resonance in the relative THz reflected field ratios (below T_c divided by above T_c) for $YBa_2Cu_3O_{6.5}$.

[1] S. I. Schlachter, U. Tutsch, W. H. Fietz, *et al*., "Pressure effect and specific heat of $RBa_2Cu_3O_x$ at distinct charge carrier concentrations: Possible influence of stripes", Int. J. Mod. Phys. B **14**, 3673 (2000).

DOI: 10.1038/NMAT3963

The equilibrium optical properties were characterized by THz time-domain spectroscopy. Single-cycle THz pulses (20-85 cm^{-1}) were focused onto the sample surface at 30° incidence, with polarization perpendicular to the Cu-O planes. The reflected electric field was measured by electro-optic sampling at different temperatures, below and above T_c.

Figure FS1.1B displays the absolute value of the frequency-dependent reflected electric field at a given temperature $|\tilde{E}_R(T)|$, normalized to the same quantity measured above T_c. Below T_c a strong edge appears ~ 30 cm^{-1}. This feature corresponds to the Josephson plasma resonance (JPR).

S2 Derivation of the complex conductivity from differential reflectivity

The transient optical properties were probed by broadband single cycle THz pulses generated in a laser-ionized plasma[2], covering a bandwidth from 20 to 500 cm^{-1}. The source was driven by 800 nm pulses with 1 mJ energy and 35 fs duration from a 2 kHz Ti:sapphire laser. The broadband THz pulses were polarized along the c-axis of the $YBa_2Cu_3O_{6.5}$ single crystal. The out-of-plane optical properties were measured at normal incidence. Mid-infrared pump pulses with a wavelength of 15 μm, 300 fs duration, and pulse energies of 8 μJ were generated by optical parametric amplification and subsequent difference frequency generation in GaSe[3].

The transient optical properties were also probed in reflection between 20 and 85 cm^{-1} by narrowband THz pulses, which were generated by optical rectification of 800 nm femtosecond pulses from a 1 kHz Ti:sapphire laser in a ZnTe crystal. The reflected pulses were electro-optically sampled by 800 nm pulses in a second ZnTe crystal. For the frequency range where the two different THz probe setups overlap, a good agreement of the transient optical constants was found, with a better signal-to-noise ratio for the data obtained from the narrowband THz probe setup.

The pump-induced change in the reflected field was measured at each time delay τ during the dynamically evolving response of the material. For each τ the relative delay between excitation and sampling pulse was kept fixed, and the THz transient was scanned with respect to these two, changing the internal delay t. Therefore each point in the THz profile probed the material at the same time delay τ after excitation.

---

[2] I.-C. Ho, X. Guo, and X.-C. Zhang, "Design and performance of reflective terahertz air-biased-coherent-detection for time-domain spectroscopy," *Opt. Express* **18,** 2872 (2010).

[3] C. Manzoni, M. Först, H. Ehrke, et al, "Single-shot detection and direct control of carrier phase drift of midinfrared pulses," *Opt. Lett.* **35,** 757 (2010).

Note that with this method, the time resolution is not determined by the intensity envelope of the THz transient, which is generally frequency-chirped and can be > 1 ps long, but by the Fourier limit of the pulse, i.e. the bandwidth.

Figure FS2.1 shows a schematic of such a two-dimensional measurement, for which the time coordinate τ defines the instant in time of the sample dynamics and the time coordinate t defines its spectral properties.

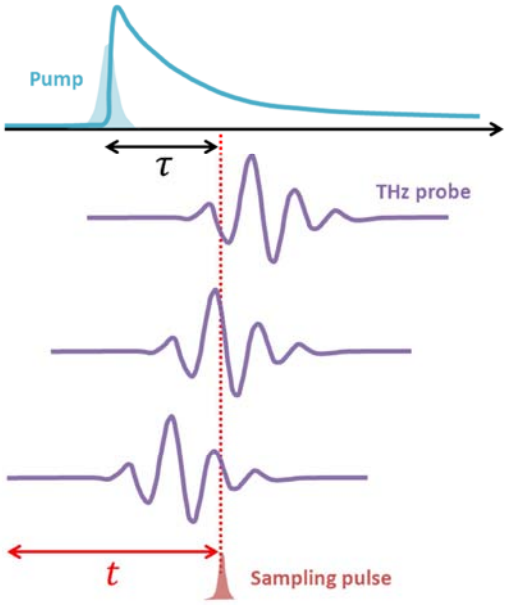

Figure FS2.1 Measurement of the time and frequency dependent THz response at a single time delay τ during the materials dynamics. A mid-infrared pulse (blue) triggers the dynamics in the $YBa_2Cu_3O_{6.5}$ sample. The spectral response at each time delay τ is obtained by fixing the delay between pump pulse and electro-optic sampling pulse (red) and by scanning the THz transient (purple) across it (t). The transient is Fourier transformed to obtain the frequency dependent response.

The quantity $\Delta E_R(t,\tau) = E_R^{pumped}(t,\tau) - E_R^{unpumped}(t,\tau)$ was acquired directly at each time delay τ by filtering the electro-optic sampling signal with a lock-in amplifier, triggered by modulation of the mid-infrared pump with a mechanical chopper. This measurement yielded "pump on" *minus* "pump off" reflected electric field.

The differential electric field $\Delta E_R(t,\tau)$ and the stationary reflected electric field $E_R(t)$ were independently Fourier transformed to obtain the complex-valued, frequency dependent $\Delta\tilde{E}_R(\omega)$ and $\tilde{E}_R(\omega)$. In those cases where the pump-induced changes to the reflected field were large enough, we also measured directly $\tilde{E}_R^{pumped}(\omega)$ and calculated the quantity $\Delta\tilde{E}_R(\omega) = \tilde{E}_R^{pumped}(\omega) - \tilde{E}_R^{unpumped}(\omega)$. The two methods yielded identical results. In order to rule out the possibility of phase drifts between $\Delta E_R(t,\tau)$

DOI: 10.1038/NMAT3963

and $E_R(t)$, we also measured these two quantities at the same time, by simultaneously modulating mid-infrared pump and THz probe and filtering the signal with two lock-in amplifiers[4].

The complex reflection coefficient of the photo-excited sample, $\tilde{r}'(\omega,\tau)$, was determined from the normalized pump-induced changes to the electric field $\Delta\tilde{E}_R(\omega,\tau)/\tilde{E}_R(\omega)$ using the relation

$$\frac{\Delta\tilde{E}_R(\omega,\tau)}{\tilde{E}_R(\omega)} = \frac{\tilde{r}'(\omega,\tau)-\tilde{r}(\omega)}{\tilde{r}(\omega)}$$

where the stationary reflection coefficient $\tilde{r}(\omega)$ was evaluated from the equilibrium optical properties[5] and our own narrow band THz time-domain spectroscopy.

Figure FS2.2A shows the normalized change in the reflected electric field transient measured as a function of sampling delay t and at a fixed pump probe time delay (maximum transient response) below and above T_c. In Figure FS2.2B we plot the time duration of the light-induced effect at 100 K (above T_c), measured by fixing the time delay t at the peak of the reflected field transient and scanning the pump-probe time-delay τ. The pump-induced dynamics after excitation is well reproduced by a double exponential decay with time constants $\tau_1 \sim 600$ fs and $\tau_2 \sim 7$ ps (see Fig. FS2.2B). Note that the slow time constant measured here is approximately the same as the one measured below T_c (see Fig. 2 and Fig. 3 in the main text).

From these measurement we extract the changes in the normal-incidence reflectivity as $\frac{\Delta R}{R}(\omega,\tau) = (|\tilde{r}'(\omega,\tau)|^2 - |\tilde{r}(\omega)|^2)/|\tilde{r}(\omega)|^2$ below and above T_c at 10 K and 100 K. They are presented in Figures FS2.2 C.1 and D.1. The measured corresponding phase changes are shown in Figures FS2.2 C.2 and D.2, respectively.

Below T_c strong reflectivity changes appear around 30 cm^{-1}. That is the frequency where the JPR is located in the equilibrium reflectivity which is indicated with a black dashed line. We find positive changes at frequencies above the JPR and negative changes at lower frequencies. The corresponding phase change of the transient reflected field evolves sharp around the shifted edge from 0 to approximately $\pi/2$.

Above T_c we observe the appearance of a reflectivity edge at 50 cm^{-1} indicative of the transient high mobility state upon photo-excitation. Also here the corresponding phase

[4] K. Iwaszczuk, D. G. Cooke, M. Fujiwara, H. Hashimoto, and P. U. Jepsen, "Simultaneous reference and differential waveform acquisition in time-resolved terahertz spectroscopy," *Opt. Expr.* **17**, 21969 (2009).

[5] C. C. Homes, T. Timusk, D. A. Bonn, et al., "Optical properties along the c-axis of $YBa_2Cu_3O_{6+x}$, for x=0.5 to 0.95: evolution of the pseudogap", *Physica C* **254**, 265 (1995).

change evolves from 0 to approximately $\pi/2$. We note that for a change on a superconduting junction one would expect a π shift of the phase. However (see S3), the transient state is an inhomogeneous state of photoexcited regions and an unperturbed background. Therefore the THz transients probe an effective medium for which the phase shift is reduced.

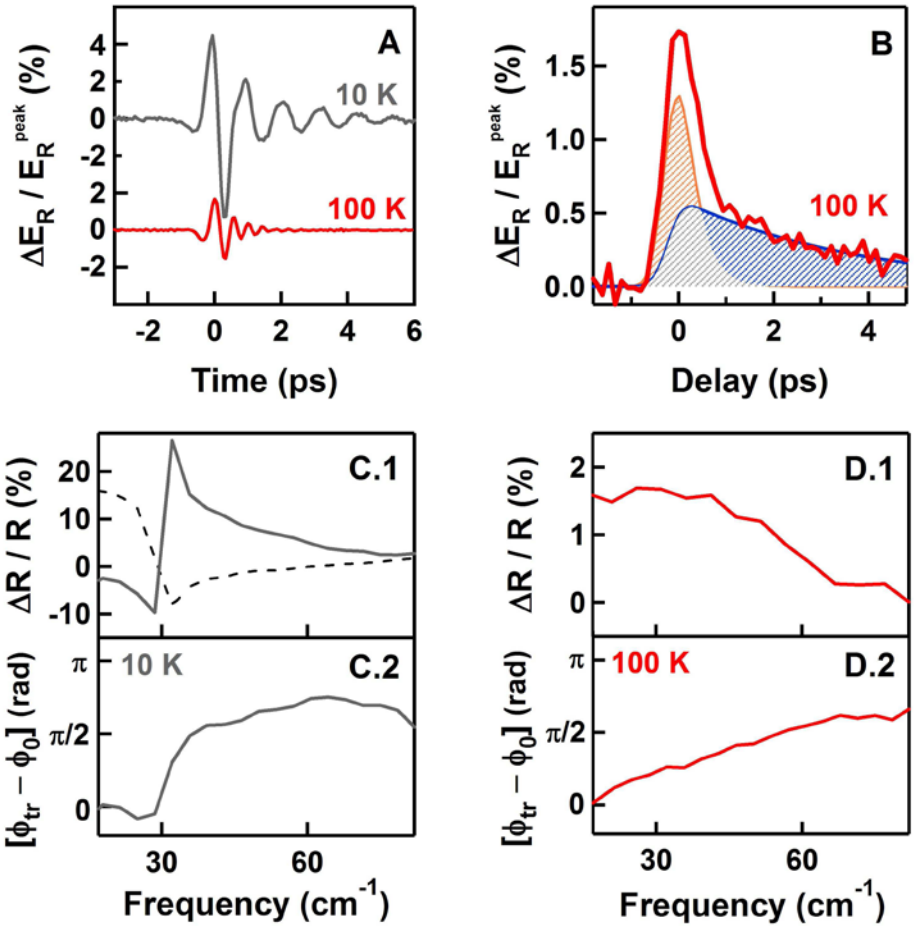

Figure FS2.2 A. Differential change in the electric field transient in $YBa_2Cu_3O_{6.5}$ at 10 K (grey) and 100 K (red). **B.** Lifetime dependence of the photo-induced effect. **C.1-D.1.** Frequency dependent differential changes of the reflectivity. **C.2-D.2.** Corresponding phase changes of the transient signal.

These "raw" reflectivity changes require reprocessing. Importantly, the measured changes above T_c are only few percent in size, due to a mismatch between the several-μm penetration depth of the probe and that of the resonant 15-μm pump, which is tuned to the middle of the *reststrahlen* band for this particular phonon and is evanescent over a few hundred nm. At low frequencies, the probe interrogates a volume that is between 10 and 20 times larger than the transformed region beneath the surface, with this mismatch being a function of frequency (see figure FS2.3).

DOI: 10.1038/NMAT3963

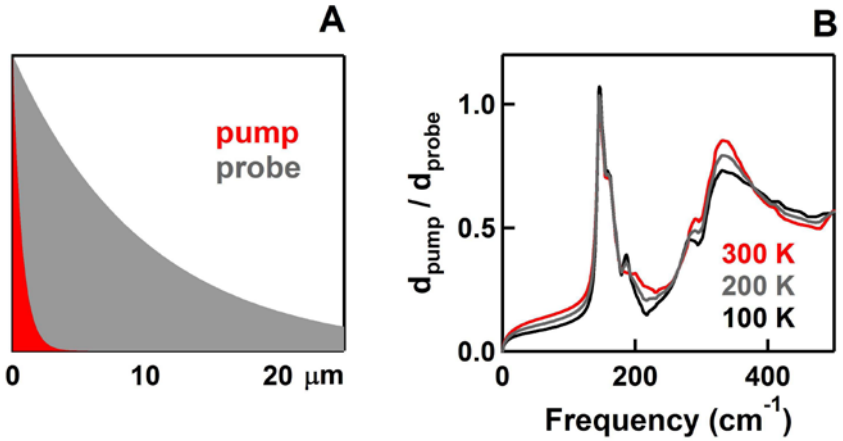

Figure FS2.3 A. Schematic of the penetration depth mismatch between resonant vibrational excitation (20-THz frequency or 15-μm wavelength, blue region) and the THz probe (grey region) in $YBa_2Cu_3O_{6.5}$. **B.** Ratio between penetration depths of pump (660 cm^{-1}) and probe (20-500 cm^{-1}).

To extract the optical constants, the penetration depth mismatch between the mid-infrared pump and the THz probe pulses was taken into account in the data analysis by assuming that the sample was photo-excited homogenously within a thickness corresponding to the mid-infrared penetration depth d, and the total reflection coefficient $\tilde{r}$ is a combined contribution from the photo-excited top layer (reflection coefficient $\tilde{r_1}$) and the non-excited bottom layer (reflection coefficient $\tilde{r_0}$)[6]

$$\tilde{r} = \frac{\tilde{r_1} + \tilde{r_0} exp(2i\delta)}{1 + \tilde{r_1}\tilde{r_0} exp(2i\delta)}$$

where $\delta = 2\pi d\,(n_1 + ik_1)/\lambda$, and λ is the wavelength of the probe pulse. The complex optical constants $\tilde{n}(\omega, \tau)$ of the photo-exited layer were obtained from a numerical solution of the above complex Fresnel equation. For the experiment with the narrowband probe pulses a 30° angle of incidence in the experimental geometry was taken into account.

From the surface refractive index, we calculate the complex conductivity for a volume that is homogeneously transformed,

$$\tilde{\sigma}(\omega, \tau) = \frac{\omega}{4\pi i}[\tilde{n}(\omega, \tau)^2 - \varepsilon_\infty],$$

[6] M. Dressel and G. Grüner, *Electrodynamics of Solids,* Cambridge University Press, Cambridge (2002).

where $\varepsilon_\infty = 4.5$, a standard value for cuprates[7].

In figure 5 in the main text the changes in the reflectivity, $\frac{\Delta R}{R}(\omega,\tau) = \big(R(\omega,\tau) - R_{eq}(\omega)\big)/R_{eq}(\omega)$, are recalculated by assuming normal-incidence reflection,

$$R(\omega) = \left|\frac{1-\tilde{n}(\omega)}{1+\tilde{n}(\omega)}\right|^2.$$

S3. Fits to the optical properties

All transient optical properties can be well explained by Bruggeman's effective medium model[8],

$$f\frac{\tilde{\varepsilon}_T(\omega)-\tilde{\varepsilon}_E(\omega)}{\tilde{\varepsilon}_T(\omega)+2\tilde{\varepsilon}_E(\omega)} + (1-f)\frac{\tilde{\varepsilon}_{eq}(\omega)-\tilde{\varepsilon}_E(\omega)}{\tilde{\varepsilon}_{eq}(\omega)+2\tilde{\varepsilon}_E(\omega)} = 0,$$

where the effective medium dielectric function $\tilde{\varepsilon}_E(\omega)$ is determined by the dielectric functions $\tilde{\varepsilon}_T(\omega)$ of the photo-susceptible region, and by the dielectric function $\tilde{\varepsilon}_{eq}(\omega)$ of the unperturbed ground state. Here Munzar's multi-layer model[9] is used to calculate $\tilde{\varepsilon}_T(\omega)$ and $\tilde{\varepsilon}_{eq}(\omega)$. Fig.FS3.1 a1-a4 shows the effective medium fit for the maximum transient response, in which a transformed volume fraction of f = 20% is used. All the transient changes are well reproduced by the fit, for example, the mixing of two superconductors (with different inter-bilayer Josephson plasma frequencies ω_{Jp1} and ω'_{Jp1}) in real space perfectly explain the plateau observed around 30 cm^{-1} in σ_2 (Fig.S3.1a1), and the small peak in $\sigma_1(\omega)$ around 50 cm^{-1} (Fig.S3.1a3).

The optical constants of the two superfluids are shown in Fig.FS3.1 b1-b4. The blue curves in Fig.FS3.1b show the part of the sample which keeps the equilibrium properties (ω_{Jp1}=110 cm^{-1}, ω_{Jp2} = 1030 cm^{-1}, 320 cm^{-1} phonon width = 40 cm^{-1})[10], and the red

[7] D. van der Marel, H. J. A. Molegraaf, J. Zaanen, et al., "Quantum critical behaviour in a high-T_c superconductor," Nature **425**, 271 (2003).

[8] Tuck C. Choy, *Effective medium theory: principles and applications*. Oxford University Press, New York, (1999).

[9] D. Munzar, C. Bernhard, A. Golnik, et al, "Anomalies of the infared-active phonons in underdoped YBCO as an evidence for the intra-bilayer Josephson effect," *Solid State Commun.* **112,** 365 (1999).

[10] The position of the Josephson plasma edges in the reflectivity, and the peaks in the loss function, are located at frequencies much smaller than ω_{Jp1} and ω_{Jp2}. Here the edge/peak positions are determined by the screened plasma frequency $\widetilde{\omega_{Jp}} = \omega_{Jp}/\sqrt{\varepsilon_\infty}$. The interband contribution shifts the peak/edge positions further to even lower frequencies than $\widetilde{\omega_{Jp}}$.

DOI: 10.1038/NMAT3963

curves show the optical properties of the photo-susceptible region (ω'_{Jp1}=310 cm^{-1} and ω'_{Jp2} = 950 cm^{-1}, 320 cm^{-1} phonon width = 4 cm^{-1}).

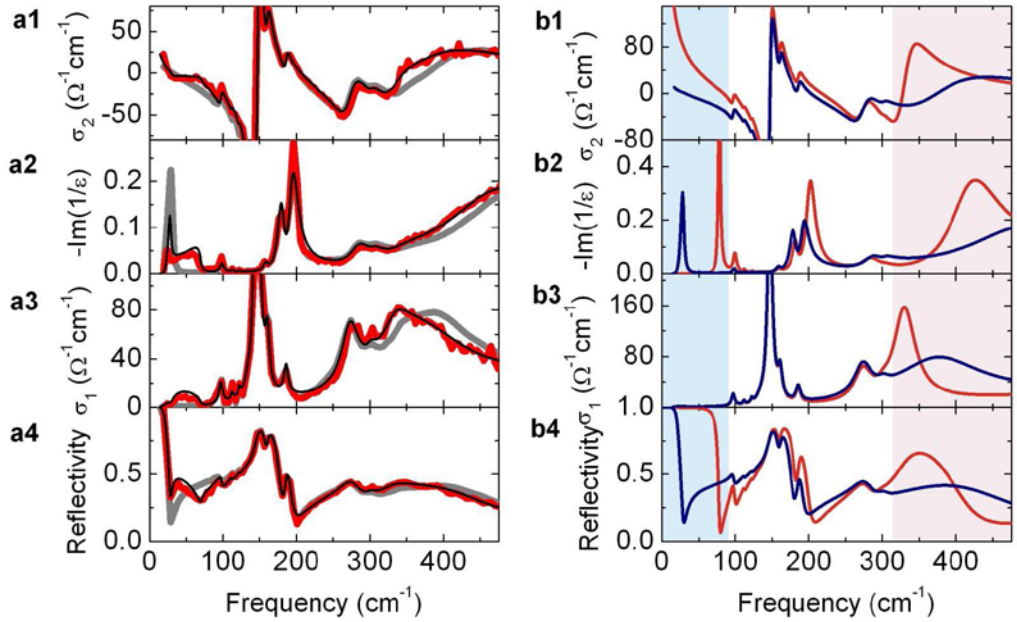

Figure FS3.1 Effective medium fit for the transient optical properties below Tc. **(a1-a4)**: equilibrium (gray), photo-excited (red), and effective medium fit (black) of the optical properties of $YBa_2Cu_3O_{6.5}$ at the maximum transient response. **(b1-b4)**: Two components used for the effective medium fit. For 20% of the photo-excited volume fraction (red), the inter-bilayer Josephson plasma frequency increases, which results in an enhanced low frequency σ_2, and a blue-shift of the inter-bilayer Josephson plasma mode from 30 to 80 cm^{-1} in the loss function and reflectivity. In the high frequency region, a reduction of the intra-bilayer Josephson plasma frequency results in a red-shift of the transverse plasma mode in σ_1, a corresponding spectral weight transfer back to the planar oxygen phonon, and a damping reduction for this phonon. 80% of the photo-excited volume retains the equilibrium properties (blue).

The transient data in the normal state (at 60 K) displays strong resemblance to the below T_c data, and can be analyzed within a similar effective medium model with a filling factor of 19%. (Fig.FS3.2). The equilibrium properties are fitted with ω_{Jp1}=0 cm^{-1}, ω_{Jp2} = 1030 cm^{-1}, and the photo-susceptible properties are fitted with ω'_{Jp1}=250 cm^{-1} and ω'_{Jp2} = 960 cm^{-1} using Munzar's multi-layer model[9].

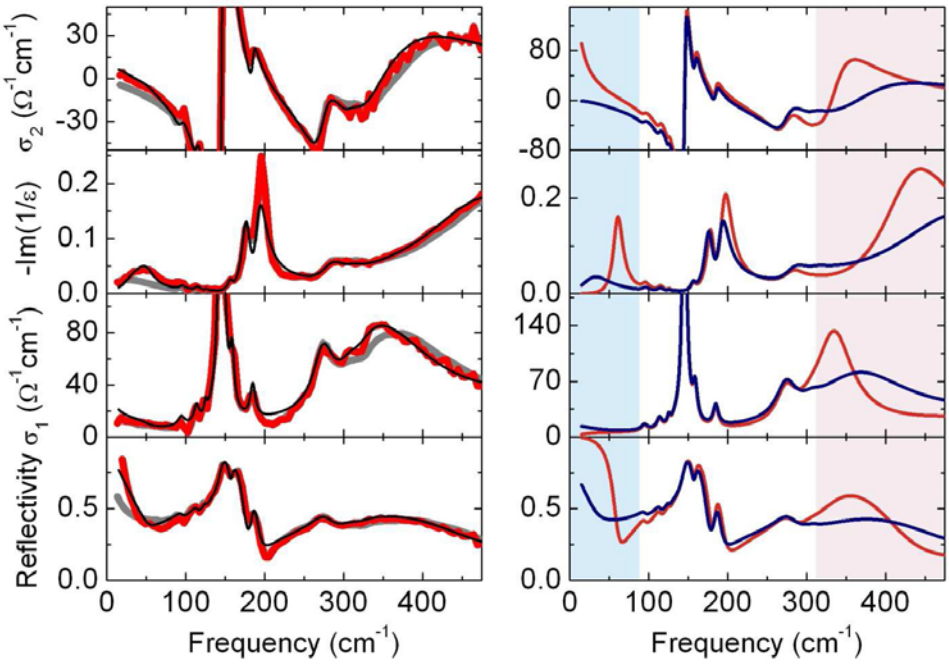

Figure FS3.2 Effective medium fit for the transient optical properties. Left panels: equilibrium (gray), photo-excited (red), and effective medium fit (black) of the optical properties of $YBa_2Cu_3O_{6.5}$ at the maximum transient response. Right panels: the two components used for the effective medium fit. A new inter-bilayer Josephson plasma mode is developed and a red-shift of the transverse plasma mode in seen in 19% of the photo-excited volume.

To calculate the two components $\tilde{\varepsilon}_T(\omega)$ and $\tilde{\varepsilon}_{eq}(\omega)$ of the effective medium fit, we also use the conventional Drude-Lorentz model[6]. As shown in Fig. FS3.3, both Munzar's multi-layer model and the Drude-Lorentz model give quantitatively comparable results for the effective medium fit.

For the conventional Drude-Lorentz fit of the below T_c data, we use ω_{Jp1} = 127 cm^{-1} to fit the low frequency Josephson plasma edge, and one Lorentz term centered at 376 cm^{-1} to fit the 400 cm^{-1} mode in σ_1. For the dielectric function $\tilde{\varepsilon}_T(\omega)$, ω'_{Jp1}=392 cm^{-1} is used to fit the enhanced superconducting response at low frequencies, and the red-shifted 400 cm^{-1} mode and the corresponding spectral weight redistribution is fitted by a Lorentz oscillator at 330 cm^{-1} with a reduced width from 144 to 35 cm^{-1}.

For the above T_c data, we use a Drude term with σ_{dc}=14 Ω^{-1}cm^{-1} and a scattering rate of Γ=25.5 cm^{-1} to fit the small metallic background at low frequency. A Lorentz term at 368 cm^{-1} is used to fit the equilibrium transverse plasma mode in σ_1. For $\tilde{\varepsilon}_T(\omega)$, we replace the low frequency Drude contribution with an inter-bilayer Josephson plasma

DOI: 10.1038/NMAT3963

mode ω'_{jp1}=297 cm^{-1}, and shift the Lorentz peak from 368 to 335 cm^{-1} and reduce its width from 151 to 55 cm^{-1} to fit the red-shift of the transverse plasma mode.

The advantage of Munzar's multi-layer model is that no additional term is needed to fit the 400 cm^{-1} mode, which comes out directly from the bilayer structure. Its frequency is mainly determined by the intra-bilayer plasma frequency ω_{jp2}, and its spectral weight is strongly coupled to the 320 cm^{-1} planar-oxygen phonon. The light-induced red-shift and the reshaping of the 400 cm^{-1} mode can be directly explained by a reduction of the intra-bilayer plasma frequency ω'_{jp2}. The sharpening of the red-shifted peak in σ_1 is results from a reduction of the 320-cm^{-1} phonon line width.

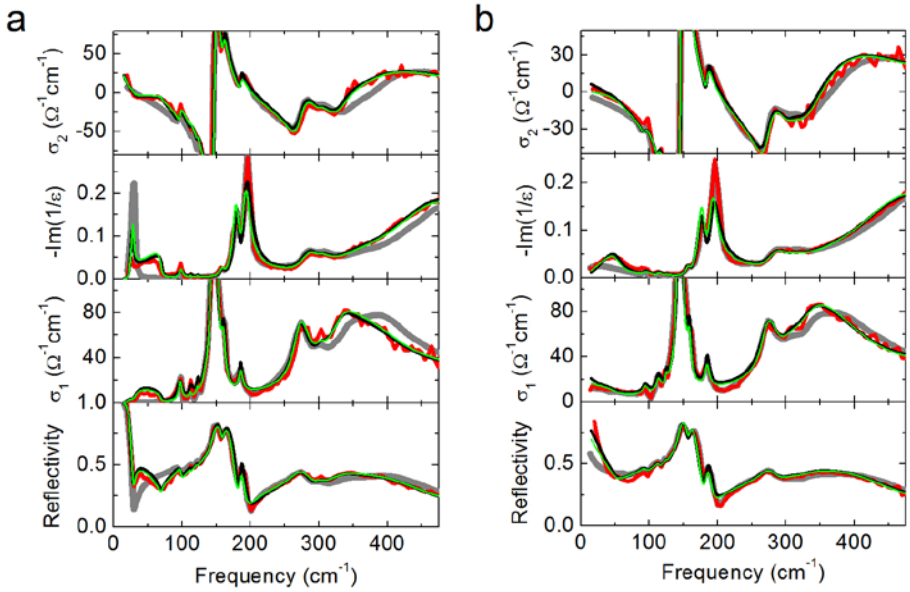

Figure FS3.3. Effective medium fit for the transient optical properties **(a)** below T_c (T = 10 K), **(b)** above T_c (T = 60 K). Equilibrium (gray), photo-excited (red), and effective medium fits from the Drude-Lorentz model (black) and from Munzar's multilayer model (green) for $YBa_2Cu_3O_{6.5}$.

Full fits to $YBa_2Cu_3O_{6.5}$ narrowband data above T_c (Fig. 5 in the main text) are shown in Figure FS3.4. Letting only the filling fraction of the high mobility state as free parameter allows describing the data at all temperatures. The photo-induced response can be fit equally well by assuming a perfect conductor with 7 ps lifetime or with infinitely long lifetime. If one assumes instead a carrier scattering time much shorter than 7 ps, for instance τ_s=1 ps, no agreement with the experimental results can be found. As shown in Figure FS3.5a, a conductor with τ_s= 1 ps and ω_{jp1}~50 cm^{-1} would display, unlike the

measured transient state, a significant increase in $\sigma_1(\omega)$ over the whole measured range, no low-frequency divergence in $\sigma_2(\omega)$, and no clear reflectivity edge.

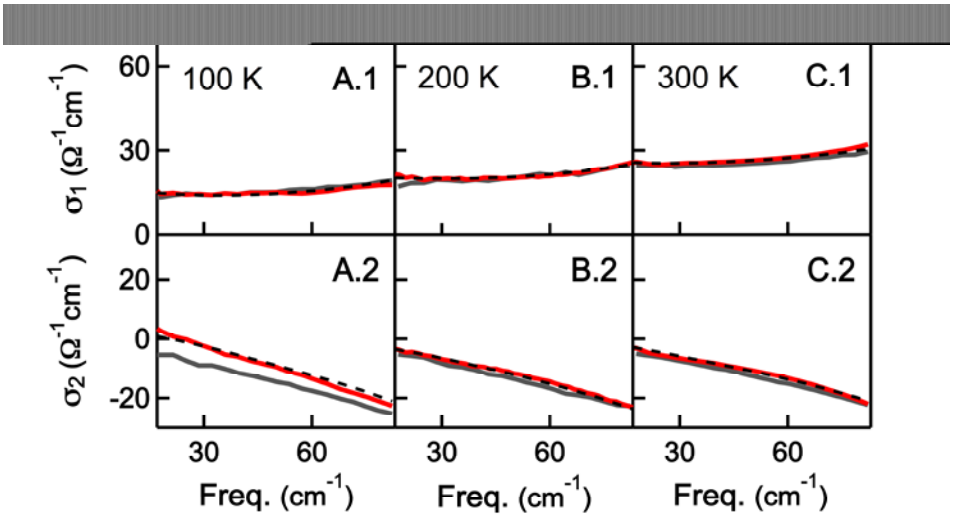

Figure FS3.4: Transient optical properties of $YBa_2Cu_3O_{6.5}$ at maximum transient response (red lines) at three temperatures: **(A)** 100 K, **(B)** 200 K, and **(C)** 330 K. The volume fraction of coherent conductor was extracted from effective medium fits to the optical properties (black dashed lines).

The lifetime of the transient state decreases with increasing temperature, down to ~2 ps at room temperature. We find that the transient optical properties remain consistent with a state in which its scattering rate is limited only by the lifetime of the state itself. Also a small increase (< 10%) in the σ_1 (ω) of the normal state conductivity was necessary for the fit. Such a small Ohmic component suggests that incoherent carriers are also being excited.

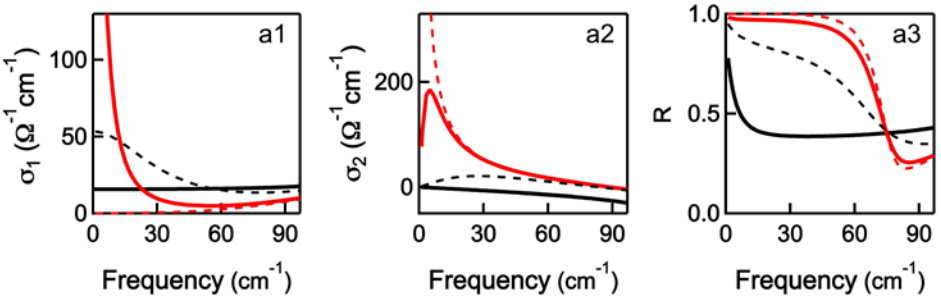

Figure FS3.5 (a1-a3) Optical properties of the equilibrium material (black lines), a conductor with infinite (red dashed line), 7 ps (red lines), and 1 ps (black dashed line) carrier scattering time, calculated with the Drude-Lorentz model.

S4 Wavelength dependence

Figure FS4.1 shows the pump wavelength dependence of the 1-THz imaginary conductivity in photo-excited $YBa_2Cu_3O_{6.5}$. This quantity, which is proportional to the

DOI: 10.1038/NMAT3963

strength of the transient high mobility state, follows the apical oxygen phonon resonance (dashed curve), and correlates almost exactly with it when the line shape is convolved with the pump pulse bandwidths (blue line). Note that measurements could not be performed at longer wavelengths than 16 μm with our optical parametric amplifier.

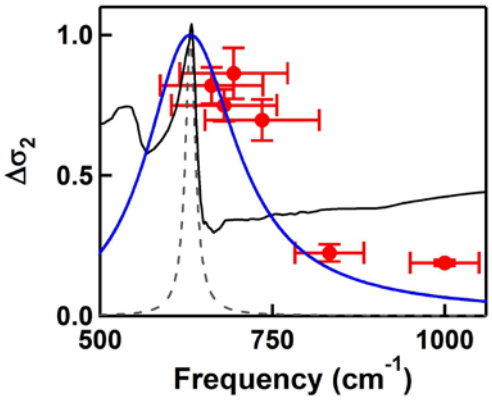

Figure FS4.1: Normalized $\Delta\sigma_2$ at 1 THz plotted as a function of pump wavelength (red dots) and measured at constant pump fluence. The horizontal bars indicate the pump spectral linewidth. The black line describes the equilibrium optical conductivity of $YBa_2Cu_3O_{6.5}$. The resonant frequency of the apical oxygen mode is indicated in the dashed black curve, and in the blue curve when convolved with the pump pulse frequency bandwidth.

S5 Evaluation of the peak lattice distortion

For these electric fields, the amplitude of the field-induced atomic displacement due to mid-infrared photo-excitation can be estimated assuming an ionic bonding between the apical O^{2-} ion and the Cu(1) ion in the CuO chains.

The atomic polarizability can be derived as $\boldsymbol{P}(\omega_0) = \varepsilon_0\chi(\omega_0)\boldsymbol{E}(\omega_0)$, where $\omega_0 = 20$ THz and $\|\boldsymbol{E}(\omega_0)\| \cong 3$ MV/cm. The susceptibility $\chi(\omega_0)$ is calculated from the c-axis equilibrium optical conductivity using $|\varepsilon_0\chi(\omega_0)| = \left|\frac{\sigma(\omega_0)}{\omega_0}\right|$. As $|\sigma_1(\omega_0)| \cong |\sigma_2(\omega_0)| \cong 30\ \Omega^{-1}\mathrm{cm}^{-1}$ (from data in Refs. 5 and 6), one gets $|\varepsilon_0\chi(\omega_0)| \cong 2\cdot 10^{-12}\Omega^{-1}\mathrm{cm}^{-1}\mathrm{s}$ and $\|\boldsymbol{P}(\omega_0)\| \cong 6\cdot 10^{-6}\ \mathrm{C}\cdot\mathrm{cm}^{-2}$.

The average size of the photo-induced electric dipole, i.e., the displacement of the oxygen ions, is then given by $d = \|\boldsymbol{P}(\omega_0)\|/nQ$, where n is the density of dipoles (2 per unit cell of volume 173 Å^3) and $Q = 3e$. This yields $d \sim 10$ pm, which is approximately 5% of the equilibrium Cu-O distance.